The Journal of Chemical Physics ARTICLE scitation.org/journal/jcp

Unified polarizable electrode models for open and closed circuits: Revisiting the effects of electrode polarization and different circuit conditions on electrode–electrolyte interfaces

Cite as: J. Chem. Phys. 157, 014111 (2022); doi: 10.1063/5.0093095
Submitted: 25 March 2022 • Accepted: 16 June 2022 •
Published Online: 6 July 2022

Ken Takahashi,[1] Hiroshi Nakano,[1,2,a)] and Hirofumi Sato[1,2,3]

AFFILIATIONS

[1] Department of Molecular Engineering, Graduate School of Engineering, Kyoto University, Kyoto 615-8246, Japan
[2] Elements Strategy Initiative for Catalysts and Batteries, Kyoto University, Kyoto 615-8245, Japan
[3] Fukui Institute for Fundamental Chemistry, Kyoto University, Kyoto 606-8103, Japan

[a)] **Author to whom correspondence should be addressed:** hnaka@moleng.kyoto-u.ac.jp

ABSTRACT

A precise understanding of the interfacial structure and dynamics is essential for the optimal design of various electrochemical devices. Herein, we propose a method for classical molecular dynamics simulations to deal with electrochemical interfaces with polarizable electrodes under the open circuit condition. Less attention has been given to electrochemical circuit conditions in computation despite being often essential for a proper assessment, especially comparison between different models. The present method is based on the chemical potential equalization principle, as is a method developed previously to deal with systems under the closed circuit condition. These two methods can be interconverted through the Legendre transformation so that the difference in the circuit conditions can be compared on the same footing. Furthermore, the electrode polarization effect can be correctly studied by comparing the present method with conventional simulations with the electrodes represented by fixed charges, since both of the methods describe systems under the open circuit condition. The method is applied to a parallel-plate capacitor composed of platinum electrodes and an aqueous electrolyte solution. The electrode polarization effects have an impact on the interfacial structure of the electrolyte solution. We found that the difference in circuit conditions significantly affects the dynamics of the electrolyte solution. The electric field at the charged electrode surface is poorly screened by the nonequilibrium solution structure in the open circuit condition, which accelerates the motion of the electrolyte solution.

I. INTRODUCTION

Understanding electrochemical interfaces at an atomic level is essential not only from the viewpoint of the fundamental chemistry but also for developing novel devices used as batteries or electric double-layer capacitors (EDLCs). EDLCs are promising energy devices,[1–4] storing charges at the interfaces through the adsorption of electrolyte ions. For optimization of the material and device design, it is necessary to clarify both equilibrium and nonequilibrium properties, including the structure of the electrolyte solution and the dynamics of charging and discharging at the interface. Molecular dynamics (MD) simulations, especially classical simulations using empirical force fields, have been widely applied to EDLC systems.[5–23] They have revealed, for example, details about the interfacial structures of ionic liquids[5–12,14,15] and aqueous electrolytes,[16–22] the capacitive properties, and operating mechanisms.[23,24] Studies on nonequilibrium dynamics, such as the response of the electrolyte to changes in the total charge or potential

of the electrode and the adsorption rate of electrolyte ions,[25–34] are also underway.

In some of these studies, charged electrodes were modeled with a fixed (nonpolarizable) charge density or atomic charges on the electrode surface[14,16,18,25,35–38] (hereafter referred to as the constant σ scheme). This absence of electrode local polarization, however, often leads to severe problems. An alternative approach is the constant potential scheme developed by Siepmann and Sprik,[39] which was later extended to the constant potential difference scheme (hereafter referred to as the constant ΔV scheme) by Reed *et al.* for studying double electrode systems.[5,6] This scheme controls the electrode potential and naturally incorporates the effects of electrode polarization, i.e., charge fluctuations on the electrode surface in response to a chemical event and thermal motions of the electrolyte solution. It may be stated that classical MD simulations with the constant ΔV scheme are now the standard for studying charged capacitors at atomic scales.

In such a situation, the effects of electrode polarization at the electrode–electrolyte interface have been discussed so far by comparing the results of the constant σ and constant ΔV schemes.[10,12,16,32,40–42] For example, Merlet *et al.* reported that an ionic liquid electrolyte at the interface is strongly stabilized due to electrode polarization in a constant ΔV simulation. The interfacial distribution of ions is significantly enhanced compared to that of constant σ simulations.[12] Inagaki and Nagaoka compared a discharging process under constant σ and ΔV conditions and concluded that the relaxation dynamics under a constant σ condition is significantly faster.[32] However, an assessment of the electrode polarization effects through such a comparison can still be improved, as the two schemes describe different electrochemical conditions: the open and closed circuit conditions. In the constant σ simulations, the total charge of each electrode is constant, corresponding to an open circuit. On the other hand, the total charge of each electrode varies under a constant ΔV condition as in a closed circuit. Therefore, a method is needed to model polarizable electrodes under the open circuit condition to correctly understand the electrode polarization effects and the difference between the open and closed circuit conditions. Although less attention may have been given to open circuit systems in electrochemistry, important experimental measurements are conducted under the open circuit condition (coulostatic condition), such as the laser-induced potential transient[43–47] and open circuit potential transient measurements.[48–50] In the former, a laser is irradiated on the electrode film via a dielectric to increase the local temperature of the electrode, and then the nonequilibrium response of the electrochemical system is investigated. In the latter, collisions of nanoparticles or emulsion droplets with the electrode surface and the growth of an oxide layer on bismuth in acid solutions are detected by measuring the electrode potential transients. It should be mentioned that Dufils *et al.* recently developed a method for treating a polarizable electrode under the open circuit condition by using the finite field method and succeeded in developing an atomistic simulation of an amperometry measurement process.[51,52]

In this study, we develop a method to model polarizable electrodes so that the total charge of each electrode is constant (referred to as the constant q method hereafter) and, then, apply the method to open circuit systems. The method is derived through the chemical potential equalization scheme,[53–56] with which the constant ΔV (= $-\Delta\mu$, minus the chemical potential difference) method was formulated in our previous work.[57] Note that this constant q formulation is essentially the same as that of the charge equilibration (QEq) method used to model polarizable molecules and metal clusters.[54,58–60] The derivation shows that the constant q and ΔV schemes can be interconverted through a Legendre transformation with respect to a control variable. This indicates that a fair comparison of the open and closed circuit conditions can be made with our unified polarizable electrode models. The electrode polarization effects can also be appropriately studied by comparing the results from our constant q and conventional constant σ simulations.

II. THEORY

We assume a system composed of two metal electrodes and an electrolyte solution between the electrodes. The total energy of the system is formally written as

$$\begin{aligned} E(\boldsymbol{q}^{\mathrm{etrd}};\boldsymbol{r}^{\mathrm{elyt}}|q_{\mathrm{L}}^{\mathrm{etrd}},q_{\mathrm{R}}^{\mathrm{etrd}}) &= E^{\mathrm{etrd}}(\boldsymbol{q}^{\mathrm{etrd}};\boldsymbol{r}^{\mathrm{elyt}}|q_{\mathrm{L}}^{\mathrm{etrd}},q_{\mathrm{R}}^{\mathrm{etrd}}) \\ &\quad + E^{\mathrm{etrd-elyt}}(\boldsymbol{q}^{\mathrm{etrd}};\boldsymbol{r}^{\mathrm{elyt}}) \\ &\quad + E^{\mathrm{elyt}}(\boldsymbol{r}^{\mathrm{elyt}}) + U^{\mathrm{nonele}}(\boldsymbol{r}^{\mathrm{elyt}}), \end{aligned} \tag{1}$$

where the first, second, third, and last terms on the right-hand side represent the electrode internal energy, the electrostatic interaction energy between the electrode and the electrolyte solution, the internal energy of the electrolyte solution, and the nonelectrostatic interaction in the system, respectively. $\boldsymbol{q}^{\mathrm{etrd}} = (q_1^{\mathrm{etrd}}, q_2^{\mathrm{etrd}}, \ldots, q_{N_{\mathrm{L}}+N_{\mathrm{R}}}^{\mathrm{etrd}})$ denotes a collection of atomic charges on the electrodes, where N_{L} and N_{R} are the number of atoms in the left and right electrodes, respectively. The total charges of the left and right electrodes, $(q_{\mathrm{L}}^{\mathrm{etrd}}, q_{\mathrm{R}}^{\mathrm{etrd}})$, are given by

$$\sum_{i\in\mathrm{L}}^{N_{\mathrm{L}}} q_i^{\mathrm{etrd}} = q_{\mathrm{L}}^{\mathrm{etrd}}, \quad \sum_{i\in\mathrm{R}}^{N_{\mathrm{R}}} q_i^{\mathrm{etrd}} = q_{\mathrm{R}}^{\mathrm{etrd}}. \tag{2}$$

As shown below, they are treated as control variables for specifying the charging states of the electrodes. We list (1) dynamical variables that will be determined variationally, (2) variables such as $\boldsymbol{r}^{\mathrm{elyt}}$ on which the function parametrically depend, and (3) the control variables in parentheses for the energy functions. They are separated with a semicolon and a vertical bar. The energy of the polarizable electrodes is modeled using the following equation:

$$E^{\mathrm{etrd}}(\boldsymbol{q}^{\mathrm{etrd}};\boldsymbol{r}^{\mathrm{elyt}}|q_{\mathrm{L}}^{\mathrm{etrd}},q_{\mathrm{R}}^{\mathrm{etrd}}) = E_0^{\mathrm{etrd}} + \sum_{i\in\mathrm{L,R}}^{N_{\mathrm{L}}+N_{\mathrm{R}}} \chi_i^{\circ} q_i^{\mathrm{etrd}} + \frac{1}{2}\sum_{i,j\in\mathrm{L,R}}^{N_{\mathrm{L}}+N_{\mathrm{R}}} q_i^{\mathrm{etrd}} J_{ij}^{\circ} q_j^{\mathrm{etrd}}, \tag{3}$$

where E_0^{etrd} is the sum of energies of isolated electrode atoms, χ_i° is the electronegativity of the electrode atom i, and J_{ij}° is the interaction kernel between the electrode atomic charges. The diagonal elements of the $\{J_{ij}^{\circ}\}$ matrix are the chemical hardness of the electrode atoms ($J_{ii}^{\circ} = U_i^{\circ}$). We assume hereafter that both the electrodes are composed of the same metal atoms; thus, $\chi_i^{\circ} = \chi^{\circ}$ and $U_i^{\circ} = U^{\circ}$. The

electrostatic interaction energy between the electrode and electrolyte solution is written as

$$E^{\text{etrd-elyt}}(\boldsymbol{q}^{\text{etrd}};\boldsymbol{r}^{\text{elyt}}) = \sum_{i\in \text{L,R}}^{N_\text{L}+N_\text{R}} \sum_{a\in\text{elyt}}^{N_\text{elyt}} q_i^{\text{etrd}} D_{ia} q_a^{\text{elyt}}, \tag{4}$$

where q_a^{elyt} is the charge of the ath atom of the electrolyte solution and D_{ia} is the interaction kernel between the ith electrode atom and the ath atom of the electrolyte solution. The internal energy of the electrolyte solution E^{elyt} is modeled with an empirical force field as in most classical MD simulations. The reader may refer to our previous works for its specific representation.[21,57]

The dynamical variables $\boldsymbol{q}^{\text{etrd}}$ are determined variationally at each $\boldsymbol{r}^{\text{elyt}}$ by minimizing the total energy with appropriate constraint conditions that specify simulation conditions (constant q or constant ΔV). In order to constrain the total charge on each electrode and to perform simulations under the constant q condition, the following objective function is introduced:

$$\mathscr{L}(\boldsymbol{q}^{\text{etrd}};\boldsymbol{r}^{\text{elyt}}|q_\text{L}^{\text{etrd}},q_\text{R}^{\text{etrd}}) = E(\boldsymbol{q}^{\text{etrd}};\boldsymbol{r}^{\text{elyt}}|q_\text{L}^{\text{etrd}},q_\text{R}^{\text{etrd}}) + \mu_\text{L}\left(\sum_{i\in\text{L}}^{N_\text{L}} q_i^{\text{etrd}} - q_\text{L}^{\text{etrd}}\right) + \mu_\text{R}\left(\sum_{i\in\text{R}}^{N_\text{R}} q_i^{\text{etrd}} - q_\text{R}^{\text{etrd}}\right), \tag{5}$$

with μ_L and μ_R being Lagrange multipliers. They are also the chemical potentials of electrons of the left and right electrodes, respectively, since

$$\partial\mathscr{L}/\partial q_i^{\text{etrd}} = 0 \;\Rightarrow\; \mu_\text{X} = -\partial E/\partial q_i^{\text{etrd}} \quad (i\in\text{X},\ \text{X}=\text{L,R}), \tag{6}$$

indicating that the chemical potentials on the atoms are equalized in each electrode. Note that q_L^{etrd} and q_R^{etrd} should be chosen so that the total system becomes charge neutral. The variational equation (6) results in the following equations for the atomic charges:

$$q_i^{\text{etrd}} = -\frac{1}{U^\circ}(\chi^\circ + v_i + \mu_\text{X}) \quad (i\in\text{X},\ \text{X}=\text{L,R}), \tag{7}$$

where v_i is the electrostatic potential acting on the ith electrode atom,

$$v_i = \sum_{j(\neq i)\in\text{L,R}}^{N_\text{L}+N_\text{R}} J_{ij}^\circ q_j^{\text{etrd}} + \sum_{a\in\text{elyt}}^{N_\text{elyt}} D_{ia} q_a^{\text{elyt}}. \tag{8}$$

The constraint condition for the total charge [or the equalization of the chemical potential in Eq. (6)] for each electrode leads to

$$\mu_\text{X} = -\left(\chi^\circ + \bar{v}_\text{X} + U^\circ \frac{q_\text{X}^{\text{etrd}}}{N_\text{X}}\right) \quad (i\in\text{X},\ \text{X}=\text{L,R}), \tag{9}$$

where $\bar{v}_\text{X} = \sum_{i\in\text{X}}^{N_\text{X}} v_i/N_\text{X}$. If we introduce the effective electrostatic potential v_i^{eff} that includes the self-term as

$$v_i^{\text{eff}} = v_i + U^\circ q_i^{\text{etrd}}, \tag{10}$$

the chemical potentials can also be written as

$$\mu_\text{X} = -(\chi^\circ + \bar{v}_\text{X}^{\text{eff}}) \quad (i\in\text{X},\ \text{X}=\text{L,R}), \tag{11}$$

where $\bar{v}_\text{X}^{\text{eff}} = \sum_{i\in\text{X}}^{N_\text{X}} v_i^{\text{eff}}/N_\text{X}$. Since here we assume $\chi_i^\circ = \chi^\circ$ for all i, the equalization of the chemical potential in Eq. (6) is reduced to the following equation of the equalization of the effective electrostatic potential:

$$v_i^{\text{eff}} = \bar{v}_\text{X}^{\text{eff}} \quad (i\in\text{X},\ \text{X}=\text{L,R}). \tag{12}$$

This equation should not be confused with the constant potential condition. The potential $\bar{v}_\text{X}^{\text{eff}}$ or μ_X (and also $\Delta\bar{v}^{\text{eff}} = \bar{v}_\text{L}^{\text{eff}} - \bar{v}_\text{R}^{\text{eff}}$ or $\Delta\mu = \mu_\text{L} - \mu_\text{R}$) fluctuates and is not constant during the simulation.

As shown in our previous work, the formulation for the constant ΔV scheme to describe polarizable electrodes in closed circuits can be derived by changing the control variables from $(q_\text{L}^{\text{etrd}}, q_\text{R}^{\text{etrd}})$ to $(q_{\text{tot}}^{\text{etrd}}, \Delta V)$ with $q_{\text{tot}}^{\text{etrd}} = q_\text{L}^{\text{etrd}} + q_\text{R}^{\text{etrd}}$ and $\Delta V = -\Delta\mu$ in a partial Legendre transformation, followed by constructing another objective function.[61] It is worth restating that both the constant q and ΔV schemes can be derived in a unified manner based on the chemical potential equalization principle and be straightforwardly interconverted via a Legendre transformation.

III. COMPUTATIONAL DETAILS

In the present work, we compare the results of the simulations on a simple double-layer capacitor under our constant q and ΔV and conventional constant σ conditions. The system is a slab composed of NaCl aqueous electrolyte solution confined between a pair of Pt electrodes. Each electrode models a Pt(111) surface of six layers. Each layer is composed of 56 Pt atoms. The lattice constant is 3.924 Å. The surfaces of the electrodes are parallel to the xy plane. The first layer of the left and right electrodes, which are exposed to the electrolyte solution, is located at $z = 0.0$ Å and $z = 50.0$ Å, respectively. The simulation cell is 19.42 Å in the x direction, 19.22 Å in the y direction, and 100.0 Å in the z direction. All the electrode atoms are fixed in position during the simulations. The electronegativity χ° and the chemical hardness U° are set to 5.6 eV and 8.5 eV/e^2, respectively, following our previous finding.[61] The electrostatic interactions are evaluated by the 3D Ewald summation augmented with the Yeh–Berkowitz correction.[62] The nonelectrostatic interactions between the electrodes and the electrolyte solutions are described by the 12-6 LJ potential functions. The LJ parameters of the Pt atoms are[63] $\epsilon_{\text{Pt}} = 32.63$ kJ/mol and $\sigma_{\text{Pt}} = 2.535$ Å. The aqueous electrolyte solution is modeled by 569 SPC/E water molecules[64] and 23 pairs of Na^+ and Cl^- ions, to set the molar concentration to be 2M. The LJ parameters of Na^+ and Cl^- are[65] $\epsilon_{\text{Na}^+} = 0.011\,72$ kJ/mol, $\epsilon_{\text{Cl}^-} = 0.492\,9$ kJ/mol, $\sigma_{\text{Na}^+} = 3.330$ Å, and $\sigma_{\text{Cl}^-} = 4.417$ Å.

The electrostatic interaction kernels in Eqs. (3) and (4) are given by

$$J_{ij}^\circ = \frac{1}{|\boldsymbol{r}_i^{\text{etrd}} - \boldsymbol{r}_j^{\text{etrd}}|} f(|\boldsymbol{r}_i^{\text{etrd}} - \boldsymbol{r}_j^{\text{etrd}}|/s_{ij}), \tag{13}$$

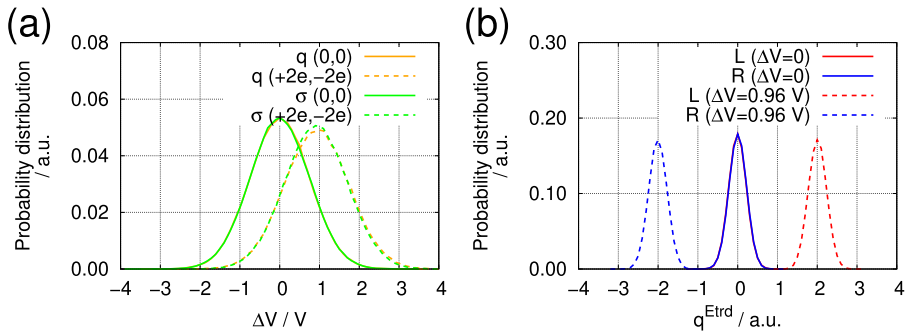

FIG. 1. (a) Probability distributions of the electrode potential difference obtained from the equilibrium simulations under the constant q (in orange) and the constant σ (in green) conditions. The results from the simulations with $(q_{\mathrm{L}}^{\mathrm{etrd}}, q_{\mathrm{R}}^{\mathrm{etrd}}) = (0,0)$ and $(q_{\mathrm{L}}^{\mathrm{etrd}}, q_{\mathrm{R}}^{\mathrm{etrd}}) = (+2e,-2e)$ are displayed with the solid and broken lines, respectively. (b) Probability distributions of the electrode total charges of the left (L) and right (R) electrodes obtained from the constant ΔV simulations with $\Delta V = 0$ V (solid lines) and $\Delta V = 0.96$ V (broken lines).

$$D_{ia} = \frac{1}{|\boldsymbol{r}_i^{\mathrm{etrd}} - \boldsymbol{r}_a^{\mathrm{elyt}}|} f(|\boldsymbol{r}_i^{\mathrm{etrd}} - \boldsymbol{r}_a^{\mathrm{elyt}}|/s_{ia}), \tag{14}$$

where $\boldsymbol{r}_i^{\mathrm{etrd}}$ and $\boldsymbol{r}_a^{\mathrm{elyt}}$ denote the coordinates of the ith electrode atom and the ath electrolyte atom, respectively. In order to circumvent the polarization catastrophe, the attenuation function $f(v)$ is introduced and modeled in this study as[66,67]

$$f(v) = \begin{cases} v^4 - 2v^3 + 2v & (v < 1), \\ 1 & (v \geq 1). \end{cases} \tag{15}$$

s_{ij} in Eqs. (13) and (14) represents the attenuation distance between the ith and jth atoms determined from[66,67]

$$s_{ij} = A(\alpha_i \alpha_j)^{1/6}. \tag{16}$$

The coefficient A is set to 2.6, and α_i is the atomic polarizability of the ith atom. The values used in this work[67–69] $\alpha_{\mathrm{H}} = 0.514$ Å^3, $\alpha_{\mathrm{O}} = 0.862$ Å^3, $\alpha_{\mathrm{Na^+}} = 0.25$ Å^3, $\alpha_{\mathrm{Cl^-}} = 3.25$ Å^3, and $\alpha_{\mathrm{Pt}} = 6.52$ Å^3. The attenuation distances then become $s_{\mathrm{Pt,Pt}} = 4.86$ Å, $s_{\mathrm{Pt,H}} = 3.18$ Å, $s_{\mathrm{Pt,O}} = 3.46$ Å, $s_{\mathrm{Pt,Na^+}} = 2.82$ Å, and $s_{\mathrm{Pt,Cl^-}} = 4.32$ Å.

Equilibrium MD calculations are carried out under six different conditions: the constant q and σ conditions with $(q_{\mathrm{L}}^{\mathrm{etrd}}, q_{\mathrm{R}}^{\mathrm{etrd}}) = (0,0)$ or $(+2e,-2e)$ and the constant ΔV condition with $\Delta V = 0$ or 0.96 V. The reason for setting $\Delta V = 0.96$ V is that it corresponds to the mean potential difference between the electrodes obtained from the constant q simulation with $(q_{\mathrm{L}}^{\mathrm{etrd}}, q_{\mathrm{R}}^{\mathrm{etrd}}) = (+2e,-2e)$ [see Fig. 1(a)]. In the constant σ simulations, all the fixed atomic charges on the electrodes are set to zero when $(q_{\mathrm{L}}^{\mathrm{etrd}}, q_{\mathrm{R}}^{\mathrm{etrd}}) = (0,0)$, but $+0.0539e(-0.0539e)$, $-0.0239e(+0.0239e)$, $+0.0068e(-0.0068e)$, and $-0.0011e(+0.0011e)$ on the first, second, third, and fourth layer of the left (right) electrodes, respectively, and zero on the fifth and sixth layers when $(q_{\mathrm{L}}^{\mathrm{etrd}}, q_{\mathrm{R}}^{\mathrm{etrd}}) = (+2e,-2e)$. These values are obtained from an equilibrium simulation under the constant q condition with $(q_{\mathrm{L}}^{\mathrm{etrd}}, q_{\mathrm{R}}^{\mathrm{etrd}}) = (+2e,-2e)$ [see Figs. 2(b) and 2(c) and Table I]. In order to obtain statistically converged results, 100 independent (uncorrelated) trajectories are obtained from both the equilibrium and nonequilibrium simulations. The initial configurations for the equilibrium simulations are prepared by extracting a snapshot every 900 ps from a 90 ns trajectory at 800 K. They are then gradually cooled down to 300 K over 4.5 ns runs. These calculations are performed with all the electrode atomic charges set to zero. A further equilibration run is carried out for each configuration under the respective condition. The final configurations of the equilibrium simulations [with $\Delta V = 0$ and $(q_{\mathrm{L}}^{\mathrm{etrd}}, q_{\mathrm{R}}^{\mathrm{etrd}}) = (0,0)$] are used as the initial configurations for the nonequilibrium simulations. For the case of nonequilibrium dynamics, we deal with a charging process. The potential difference or the total charges of the electrodes are instantaneously changed at $t = 0$ from $\Delta V = 0$ to $\Delta V = +0.96$ V

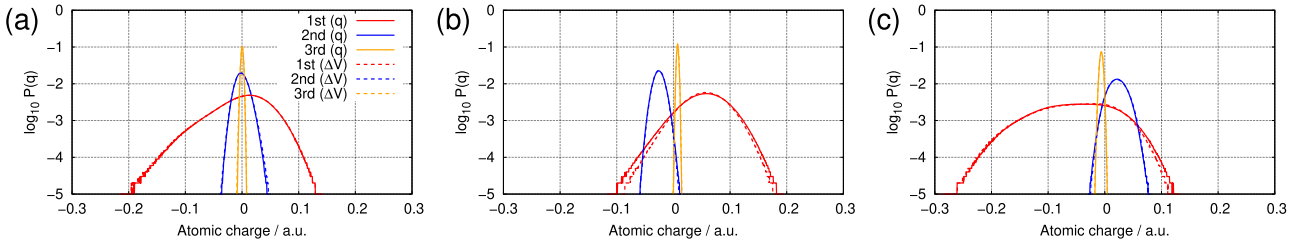

FIG. 2. Probability distributions of the atomic charges on the first, second, and third layers of the electrodes obtained from the equilibrium simulations under the constant q and ΔV conditions with (a) $(q_{\mathrm{L}}^{\mathrm{etrd}}, q_{\mathrm{R}}^{\mathrm{etrd}}) = (0,0)$ or $\Delta V = 0$ V, and (b) and (c) $(q_{\mathrm{L}}^{\mathrm{etrd}}, q_{\mathrm{R}}^{\mathrm{etrd}}) = (+2e,-2e)$ or $\Delta V = 2$ V on the left and right electrodes, respectively.

TABLE I. Mean values of charge on each electrode atom in the first three layers under the constant q condition with $(q_L^{etrd}, q_R^{etrd}) = (+2e, -2e)$ and the constant ΔV condition with $\Delta V = 0.96$ V. The values for the left and right electrode atoms are listed in this order.

	Constant q	Constant ΔV
First	$(+0.0551e, -0.0529e)$	$(+0.0552e, -0.0532e)$
Second	$(-0.0255e, +0.0223e)$	$(-0.0255e, +0.0225e)$
Third	$(+0.0075e, -0.0062e)$	$(+0.0075e, -0.0062e)$

or from $(q_L^{etrd}, q_R^{etrd}) = (0, 0)$ to $(q_L^{etrd}, q_R^{etrd}) = (+2e, -2e)$. All the production runs are carried out in the NVT ensemble at 300 K with a timestep of 3 fs. The temperature is controlled by using the Nosé–Hoover thermostat[70] with a relaxation time of 0.5 ps. This thermostat is used even in the nonequilibrium simulations since a sudden change in the total charge of the electrodes under the constant q and σ conditions significantly raises the system temperature. We verify from comparative simulations that the dependence of the dynamics on the relaxation time of the thermostat is insignificant under the present simulation conditions. The potential of mean force (PMF) profiles of ions approaching the electrode surface are calculated by integrating the mean force in the z direction. In the PMF calculations, the target ion can translate in the x and y directions but is fixed in the z direction by using the RATTLE algorithm.[71] The mean force at each place is sampled from six independent 900 ps trajectories. All the MD calculations are carried out by using our modified version of DL_POLY Classic 1.10[72] with which our constant q and ΔV schemes are implemented.

IV. RESULTS AND DISCUSSION

A. Equilibrium properties

1. Potential and charge fluctuation on the electrodes

In the constant q and σ simulations, the total charge of each electrode is constant, but the electrode potential difference fluctuates. Conversely, in the constant ΔV simulations, the total charge of each electrode fluctuates, but the electrode potential difference remains constant. Figure 1(a) displays the probability distributions of the electrode potential difference obtained from the equilibrium simulations with the total electrode charge being constant. These probability distributions produced by the constant q and σ simulations are almost the same and look like a Gaussian in the case of both $(q_L^{etrd}, q_R^{etrd}) = (0, 0)$ and $(q_L^{etrd}, q_R^{etrd}) = (+2e, -2e)$. Figure 1(b) shows the probability distribution of the total charge of the left and right electrodes produced by the equilibrium simulations under the constant ΔV condition. The total charge on each electrode fluctuates around zero when $\Delta V = 0$ and $\pm 2e$ when $\Delta V = 0.96$ V as expected.

Further insight into electrode polarization is obtained by inspecting the probability distributions of the atomic charges for each layer (from the first to the third) under the constant q and ΔV conditions as shown in Fig. 2. The average values for each layer are listed in Table I. The probability distributions and the average values obtained from the different (open and closed circuit) conditions are quite similar to each other. The asymmetric distribution of the atomic charges on the first layer, as observed in the present and previous constant ΔV simulations,[11,13,31,42,73,74] is also obtained from the constant q simulation.

2. Interfacial distribution of ions

Next, we focus on the interfacial structure of the electrolyte ions that can be affected by the electrode local polarization. The number density profiles and their running integration number profiles are illustrated in the top and middle panels of Fig. 3(a) under the constant q and σ conditions with $(q_L^{etrd}, q_R^{etrd}) = (0, 0)$ and under the constant ΔV conditions with $\Delta V = 0$ V. There are non-negligible differences in the distribution and population of Na^+ and Cl^- ions within 5 Å distance from the electrode surface between the constant σ simulation and the constant q and ΔV simulations, as expected. These differences arise from the stabilization of the adsorbed ions by the electrode local polarization present only in the constant q and ΔV simulations. The effect can be seen more clearly by calculating the PMF profiles of a Na^+ and a Cl^- ion approaching the electrode surface under the constant q and σ conditions. The difference indicates that the electrode polarization can change the adsorption distance of a Na^+ species as the PMF starts to arise at a closer distance from the surface. The PMF profile for a Cl^- species has two minima at $z = 3.4$ and 6.0 Å regardless of the presence or absence of the electrode local polarization effects. However, the effects make it easier for a Cl^- ion to approach the electrode surface with no net charge.

Charging each electrode or applying a finite electrode potential difference attracts ions of opposite charge and the peaks of the distributions become much higher as shown in the top panels in Figs. 3(b) and 3(c). The corresponding integration number profiles are also shown in the middle panels. In these simulations, the differences between the constant q, σ, and ΔV conditions seem to have small but complicated effects on the ion distributions. While the first peaks in the Cl^- distributions at the positively charged (left) electrode surface are similar to each other under all the conditions, small peaks in the Na^+ distributions emerge only in the constant q and ΔV simulations at around 2.3 Å distance from the negatively charged (right) electrode surface. These observations are consistent with the difference in the PMF profiles obtained from the constant q and σ simulations shown in the bottom panels in Figs. 3(b) and 3(c). Note that we find the distribution functions of the atoms of water molecules are similar to each other but small differences are observed especially in the highest peak heights in close proximity to the electrode surface between the constant q and ΔV simulations with $(q_L^{etrd}, q_R^{etrd}) = (+2e, -2e)$ and $\Delta V = 0.96$ V (not shown here). Such difference at the adsorbed water layer seems to affect the ion distributions further away from the electrode surface than their first peaks. These differences indicate that differences in the circuit condition could affect the interfacial structure of the electrolyte solution, though the electrode surface polarizes in almost the same way on average as shown in Fig. 2.

B. Nonequilibrium dynamics

Here, we discuss the interfacial dynamics in response to a sudden change in the total electrode charges from $(q_L^{etrd}, q_R^{etrd}) = (0, 0)$

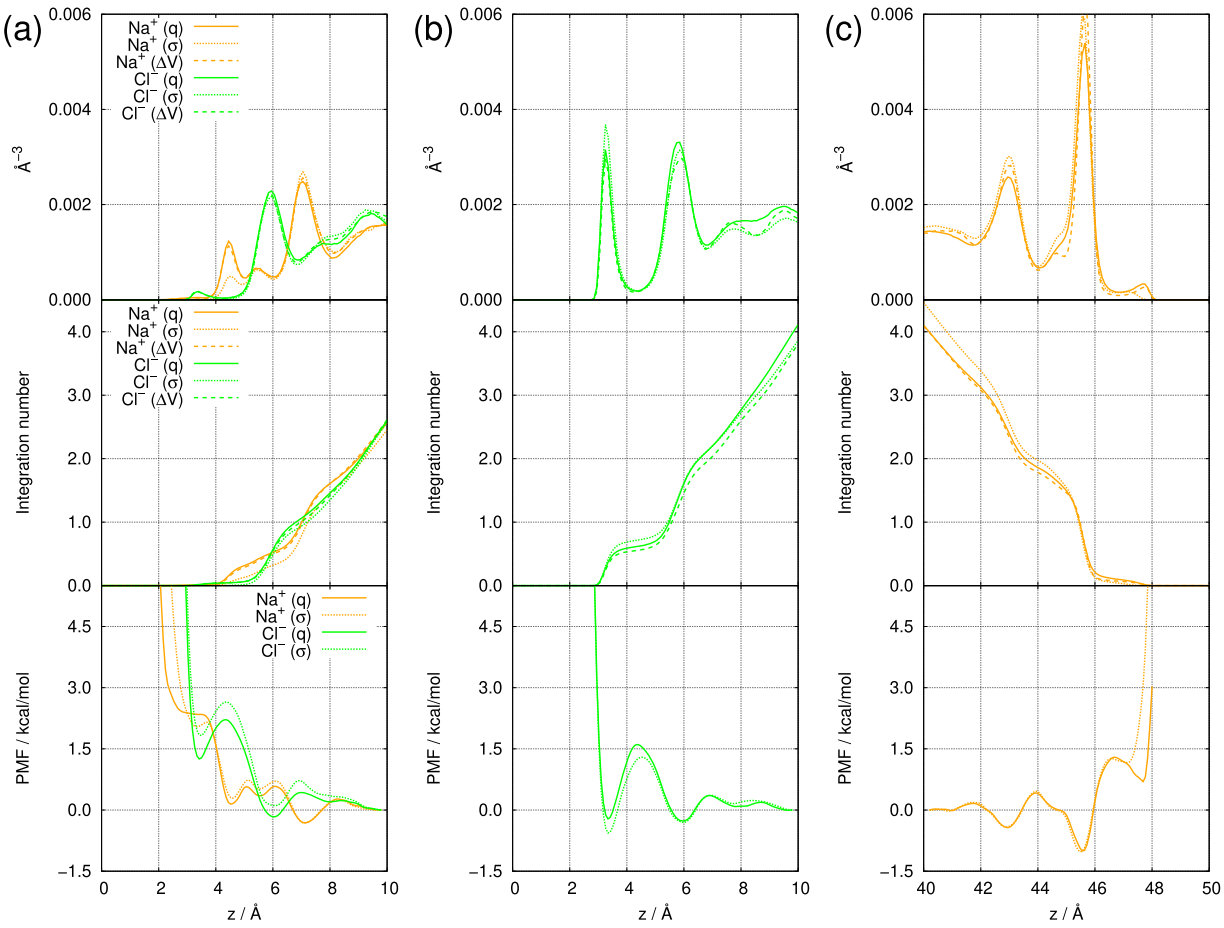

FIG. 3. Number density profiles (top panels), running integration number profiles (middle panels), and PMF profiles (bottom panels) for Na^+ (in orange) and Cl^- (in green) (a) at the electrode interfaces with $(q_L^{etrd}, q_R^{etrd}) = (0, 0)$ or $\Delta V = 0$ V, (b) and (c) at the left (positive) and right (negative) electrode interfaces, respectively, with $(q_L^{etrd}, q_R^{etrd}) = (+2e, -2e)$ or $\Delta V = 0.96$ V. The solid, dotted, and broken lines represent the results from the constant q, σ, and ΔV simulations, respectively. Only the results from the constant q and σ simulations are displayed for the PMF profiles.

to $(+2e, -2e)$ in the constant q and σ simulations, and from $\Delta V = 0$ V to 0.96 V in the constant ΔV simulation. First, it should be noted that the absolute value of the electrode total charge in the constant ΔV simulation is significantly smaller than $2e$ just after the change in electrode potential [see Fig. 4(b)] because the interfacial structure at the moment is considerably different from the equilibrium double-layer structure and the electrostatic screening is insufficient. Following previous works,[10,25,31,32] we investigate the time evolution of the electrode potential difference $\Delta\bar{v}^{\,\mathrm{eff}}(= \Delta V)$ under the constant q and σ conditions, and of the electrode total charges (q_L^{etrd}, q_R^{etrd}) under the constant ΔV condition as displayed in Fig. 4. The relaxation under the constant q condition seems almost identical with that under the constant σ condition: The electrode potential difference jumps to over 40 V at the moment of the electrode total charge switching, indicating a strong electric field is created in the cell. It, then, drops down to around 5 V with oscillations within 0.6 ps and quickly decays to around 0.96 V (the equilibrium value) within 150 ps. This similarity between the results from the constant q and σ simulations indicates that it is the change in the electrode total charge that dominates the interfacial dynamics in such a simple parallel-plate capacitor and the electrode local polarization plays a minor role. On the other hand, they are qualitatively different from the relaxation dynamics observed in the constant ΔV simulation. The total electrode charges vary by less than $\pm 0.05e$ just after the electrode potential switching, then gradually approach the equilibrium state of $(q_L^{etrd}, q_R^{etrd}) = (+2e, -2e)$ in longer than 500 ps. This slower relaxation dynamics in the closed circuit compared to that in the open circuit is consistent with those observed in different systems in which the electrolyte solutions are ionic liquids.[10,32]

We assume that these relaxation dynamics can be attributed to the rotational motion of the water molecules and the drift-diffusion motion of the ions in the cell. In order to investigate the dynamics of the water molecules at the electrode–electrolyte interface and in

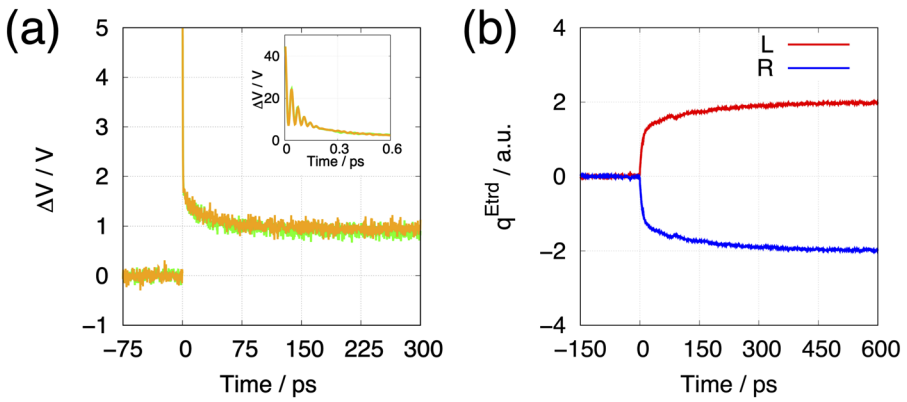

FIG. 4. (a) Time evolution of electrode potential difference ΔV under the constant q (in orange) and σ (in green) conditions, and (b) time evolution of electrode total charges ($q_{\mathrm{L}}^{\mathrm{etrd}}$ in red and $q_{\mathrm{R}}^{\mathrm{etrd}}$ in blue) under the constant ΔV condition. The electrode total charges are switched from $(q_{\mathrm{L}}^{\mathrm{etrd}}, q_{\mathrm{R}}^{\mathrm{etrd}}) = (0, 0)$ to $(+2e, -2e)$ or the electrode potential difference is switched from $\Delta V = 0$ V to 0.96 V at $t = 0$. The inset in (a) is an enlarged view of the moment of switching.

the bulk region separately, we first calculate the ensemble average of $\cos\phi_z$, i.e., $\langle\cos\phi_z\rangle$, as functions of time, where ϕ_z is the angle between the dipole moment of a water molecule and the z axis in the interfacial region within 4 Å (including only the first adsorbed water layer) from the electrode surface [Figs. 5(a) and 5(c)]. The values of $\langle\cos\phi_z\rangle$ is nearly zero at $t < 0$ since most of the interfacial water molecules are directed almost parallel to the electrode surface. They approach the new equilibrium values at large t. In the constant q and σ simulations, the value of $\langle\cos\phi_z\rangle$ jumps up just after the switching. It indicates the interfacial water molecules quickly rotate so that their dipole moments are tilted toward the z axis, the direction of the large electric field produced by the charged electrodes. The values of $\langle\cos\phi_z\rangle$ decay with oscillations mostly in about 0.6 ps, indicating that the librational motion of the water molecules is excited by the sudden switching and then quickly attenuated. The difference in the results is small between the constant q and σ conditions. In contrast, in the constant ΔV simulation, the average direction of the interfacial water molecules varies more calmly since the electric field created by the switching is much smaller than that in the constant q and σ simulations. It takes around 10 ps or more for the initial (relatively) fast relaxation to be mostly completed.

Next, we investigate the results for the bulk region shown in Fig. 5(b). The sampled water molecules are more than 10 Å away from the electrode surfaces. In the constant q and σ simulations, the water molecules are forced to be tilted toward the direction of the electric field within 0.6 ps after the switching as at the interface. They then decay exponentially in several hundred ps to be randomized in orientation. A qualitatively different relaxation dynamics is observed in the constant ΔV simulation. The water molecules initially rotate toward the z axis as those at the interface in about 10 ps, but gradually start to rotate randomly in 400 ps. The former dynamics is a manifestation of the dielectric relaxation of water molecules. The curve fitting at 0 ps $< t <$ 10 ps with an exponential function gives the time constant of 4.3 ps, in reasonable agreement with that of the dielectric relaxation (~7 ps) at 300 K.[75]

These orientational relaxations of the water molecules observed in all of the simulations last in a time scale (several hundred ps or longer) much longer than that of the dielectric relaxation of bulk water. They are thus expected to be coupled with a slower relaxation process related to the motion of the ions. Figure 6 shows the time evolution of the difference in the number of ions ($\Delta N = N_{\mathrm{Na^+}} - N_{\mathrm{Cl^-}}$) in the region within 10 Å distance from the

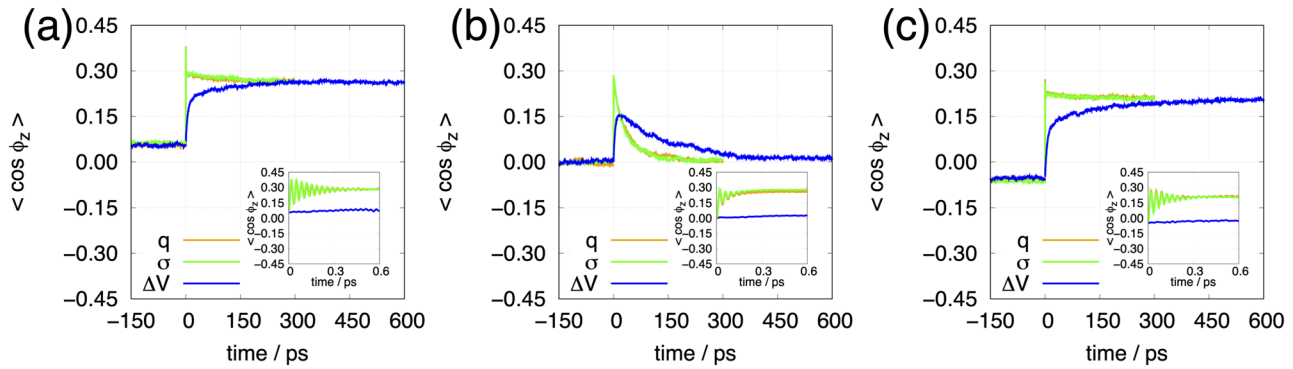

FIG. 5. Time evolution of the ensemble average of $\cos\phi_z$ with ϕ_z being the angle between the z axis in the simulation cell and the dipole moment of a water molecule. The averages are taken for the water molecules (a) within 4 Å distance from the left electrode surface, (b) more than 10 Å away from both the electrode surfaces, and (c) within 4 Å distance from the right electrode surface. The results from the constant q, σ, and ΔV simulations are depicted with orange, green, and blue lines, respectively.

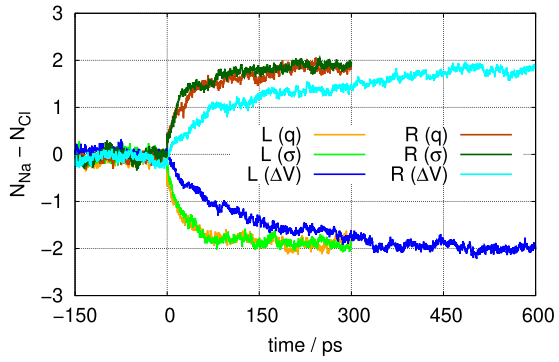

FIG. 6. Time evolution of the difference between the numbers of Na^+ and Cl^- within 10 Å distance from the left and right electrode surfaces. "L," "R," "q," "σ," and "ΔV" in the figure legends represent the left electrode interface, the right electrode interface, the constant q condition, the constant σ condition, and constant ΔV condition, respectively.

TABLE II. Time constants (in ps) obtained by fitting curves obtained from the constant q, σ, and ΔV simulations with an exponential function in the range of $t > 20$ ps. The curves represent the functions of time for the difference in the number of ions (ΔN) and the electrode potential difference or the electrode total charge (ΔV or q). The left and right figures separated with a slash represent the time constants for the process on the left and right electrodes, respectively.

	Const. σ	Const. q	Const. ΔV
ΔN	30/81	45/67	159/207
ΔV or q	30	30	160/160

electrode surfaces. The values are around zero at $t < 0$ (before the switching) since each electrode has no total charge on average in all of the simulations. They approach ±2 at large t in equilibrium as expected. The results from the constant q and σ simulations are similar to each other, and it takes less than 300 ps to reach the equilibrium value. In contrast, it takes more than 600 ps under the constant ΔV condition. These curves are fitted well with an exponential function in the range of $t > 20$ ps. The relaxation time constants for each case are listed in Table II. The smaller time constants in the open circuit (constant q and σ) systems than those in the closed circuit (constant ΔV) system come from the drift dynamics of the ions significantly accelerated by the large electric field, created by the charged electrode surfaces that are poorly screened by the nonequilibrium solution structures.

V. CONCLUSIONS

We have introduced the constant q method for classical MD simulations to describe a pair of polarizable electrodes with the total charge of each electrode being constant. This method resolves the problem of neglecting the local polarization effects of electrodes in conventional simulations that put the constant charge density (atomic charges) on the electrode surfaces (constant σ simulations). The formulation is based on the chemical potential equalization principle as that of the constant electrode potential difference (constant ΔV) method. These can be interconverted through a Legendre transformation with respect to a variable that controls the charging state of the electrodes. It, thus, enables us to compare the circuit conditions on the same footing to correctly model electrode–electrolyte interfaces in open and closed circuits with the electrode polarization effects being fully included. The electrode polarization effects themselves are also correctly studied by comparing the constant q and σ simulations.

We applied the three schemes, the constant q, σ, and ΔV schemes, to a typical parallel-plate capacitor composed of two metal electrodes and an aqueous electrolyte solution in order to investigate the effects of electrode polarization and the difference between open and closed circuit conditions on the structure and dynamics at the interface. A comparison of the constant q and σ simulations shows that the electrolyte ions are attracted more strongly to the electrode surface by the electrode local polarization. Though the electrode surfaces polarize similarly on average in the constant q and ΔV simulations, the surface structures of the electrolyte solution are slightly different even in this simple system. This result implies that not only the electrode polarization but also the circuit condition could affect the interfacial structure in microscopic systems.

The dynamics were studied through the relaxation processes after sudden switching of the total charge on each electrode or of the electrode potential difference. The fact that the difference in the results between the constant q and σ simulations is small indicates that the electrode local polarization plays a minor role in the relaxation dynamics in this system. In contrast, there is a significant difference in the relaxation times between the constant q and ΔV (the open and closed circuit) conditions, as discussed (approximately) in previous works that compare the constant σ and ΔV simulations. The relaxation dynamics under the constant q condition is considerably faster than that under the constant ΔV condition. This is because the drift motion of the ions is significantly accelerated by the large electric field produced by the charged electrodes. Under the constant ΔV condition, only a small amount of charge builds up on each electrode to realize the potential difference applied by the switching and a small electric field acts on the ions. Both the large electric field in the open circuit and the small amount of electrode charge in the closed circuit originate from the common factor that the electrode surfaces are electrostatically poorly screened by the nonequilibrium solution structures in the relaxation process.

Although the comparison between the constant q and σ simulations indicates that the effects of the electrode local polarization are small, they may have non-negligible impacts on the structure and dynamics of ions and solvent molecules intercalated in an electrode, such as a graphite electrode, since many of them can be in close proximity to the electrode surfaces. Due to the formulation being independent of the type of an electrolyte solution, the constant q method can be applied to more complex systems (as long as the electrodes are metallic) including, for example, ionic liquids in nanoporous carbon electrodes, the structure and dynamics of which have attracted much attention.[26,76–78] Use of the constant q method can pave the way for computational investigations of open circuit systems experimentally studied by laser-induced or open circuit potential transient measurements mentioned in Sec. I by controlling the electrode total charge. Furthermore, our approach unifying the constant ΔV and q methods could facilitate the understanding

of possible differences in the rapid (especially in the timescale from fs to ns) relaxation dynamics of an electric double layer[43,79] just after applying a potential or charge impulse to the electrode under closed and open circuit conditions, which could be observed by a potentiostatic method and a coulostatic method, respectively.[80] Note also that the constant ΔV and q methods can also be used to perform computational voltammetry and amperometry to study the dynamics of a capacitor modeled with double electrodes by varying the control variable ΔV or $q_{\mathrm{L}}^{\mathrm{etrd}}(=-q_{\mathrm{R}}^{\mathrm{etrd}})$ in time at a constant rate as Dufils *et al.* did with their finite field method for a single electrode system.[52] We hope that our approaches realizing classical MD simulations of capacitors or more generally electrochemical cells contribute toward unraveling the interfacial structure and dynamics occurring under different electrochemical conditions.

ACKNOWLEDGMENTS

This work was financially supported by Grant-in-Aid for Young Scientists (B) (Grant No. 18K14179) and Grant-in-Aid for Scientific Research (C). A part of this work was performed under the management of *Elements Strategy Initiative for Catalysts and Batteries (ESICB)*. K.T. acknowledges financial support from the Nikki-Saneyoshi (JGC-S) Scholarship Foundation.

AUTHOR DECLARATIONS

Conflict of Interest

The authors have no conflicts to disclose.

Author Contributions

Ken Takahashi: Conceptualization (supporting); Data curation (lead); Formal analysis (lead); Investigation (equal); Methodology (equal); Software (equal); Visualization (lead); Writing-original-draft (equal); Writing-review-editing (equal). **Hiroshi Nakano:** Conceptualization (lead); Funding acquisition (equal); Investigation (equal); Methodology (equal); Project administration (lead); Resources (equal); Software (equal); Supervision (lead); Validation (lead); Writing-original-draft (equal); Writing-review-editing (equal). **Hirofumi Sato:** Funding acquisition (equal); Resources (equal); Writing-original-draft (equal).

DATA AVAILABILITY

The data that support the findings of this study are available from the corresponding author upon reasonable request.

REFERENCES

[1] C. Schütter, S. Pohlmann, and A. Balducci, Adv. Energy Mater. **9**, 1900334 (2019).
[2] H. Shao, Y.-C. Wu, Z. Lin, P.-L. Taberna, and P. Simon, Chem. Soc. Rev. **49**, 3005 (2020).
[3] J. Vatamanu, O. Borodin, M. Olguin, G. Yushin, and D. Bedrov, J. Mater. Chem. A **5**, 21049 (2017).
[4] Z. Bo, C. Li, H. Yang, K. Ostrikov, J. Yan, and K. Cen, Nano-Micro Lett. **10**, 33 (2018).
[5] S. K. Reed, O. J. Lanning, and P. A. Madden, J. Chem. Phys. **126**, 084704 (2007).
[6] S. K. Reed, P. A. Madden, and A. Papadopoulos, J. Chem. Phys. **128**, 124701 (2008).
[7] M. K. Petersen, R. Kumar, H. S. White, and G. A. Voth, J. Phys. Chem. C **116**, 4903 (2012).
[8] S. Park and J. G. McDaniel, J. Chem. Phys. **152**, 074709 (2020).
[9] J. Vatamanu, O. Borodin, and G. D. Smith, J. Am. Chem. Soc. **132**, 14825 (2010).
[10] J. Vatamanu, O. Borodin, and G. D. Smith, J. Phys. Chem. B **115**, 3073 (2011).
[11] C. Merlet, M. Salanne, and B. Rotenberg, J. Phys. Chem. C **116**, 7687 (2012).
[12] C. Merlet, C. Péan, B. Rotenberg, P. A. Madden, P. Simon, and M. Salanne, J. Phys. Chem. Lett. **4**, 264 (2013).
[13] C. Merlet, M. Salanne, B. Rotenberg, and P. A. Madden, Electrochim. Acta **101**, 262 (2013).
[14] G. Feng, J. S. Zhang, and R. Qiao, J. Phys. Chem. C **113**, 4549 (2009).
[15] M. Buraschi, S. Sansotta, and D. Zahn, J. Phys. Chem. C **124**, 2002 (2020).
[16] H. Yang, X. Zhang, J. Yang, Z. Bo, M. Hu, J. Yan, and K. Cen, J. Phys. Chem. Lett. **8**, 153 (2017).
[17] R. K. Kalluri, D. Konatham, and A. Striolo, J. Phys. Chem. C **115**, 13786 (2011).
[18] R. K. Kalluri, T. A. Ho, J. Biener, M. M. Biener, and A. Striolo, J. Phys. Chem. C **117**, 13609 (2013).
[19] R. K. Kalluri, M. M. Biener, M. E. Suss, M. D. Merrill, M. Stadermann, J. G. Santiago, T. F. Baumann, J. Biener, and A. Striolo, Phys. Chem. Chem. Phys. **15**, 2309 (2013).
[20] Y. Matsumi, H. Nakano, and H. Sato, Chem. Phys. Lett. **681**, 80 (2017).
[21] K. Takahashi, H. Nakano, and H. Sato, J. Chem. Phys. **153**, 054126 (2020).
[22] T. Liang, A. C. Antony, S. A. Akhade, M. J. Janik, and S. B. Sinnott, J. Phys. Chem. A **122**, 631 (2018).
[23] S. Jo, S.-W. Park, C. Noh, and Y. Jung, Electrochim. Acta **284**, 577 (2018).
[24] P. Wu, J. Huang, V. Meunier, B. G. Sumpter, and R. Qiao, J. Phys. Chem. Lett. **3**, 1732 (2012).
[25] C. Pinilla, M. G. Del Pópolo, J. Kohanoff, and R. M. Lynden-Bell, J. Phys. Chem. B **111**, 4877 (2007).
[26] C. Péan, C. Merlet, B. Rotenberg, P. A. Madden, P.-L. Taberna, B. Daffos, M. Salanne, and P. Simon, ACS Nano **8**, 1576 (2014).
[27] K. Takae and A. Onuki, J. Phys. Chem. B **119**, 9377 (2015).
[28] S.-W. Park, S. Kim, and Y. Jung, Phys. Chem. Chem. Phys. **17**, 29281 (2015).
[29] C. Péan, B. Rotenberg, P. Simon, and M. Salanne, Electrochim. Acta **206**, 504 (2016).
[30] K. Xu, X. Ji, B. Zhang, C. Chen, Y. Ruan, L. Miao, and J. Jiang, Electrochim. Acta **196**, 75 (2016).
[31] C. Noh and Y. Jung, Phys. Chem. Chem. Phys. **21**, 6790 (2019).
[32] T. Inagaki and M. Nagaoka, J. Comput. Chem. **40**, 2131 (2019).
[33] B. Demir and D. J. Searles, Nanomaterials **10**, 2181 (2020).
[34] G. F. L. Pereira, E. E. Fileti, and L. J. A. Siqueira, J. Phys. Chem. C **125**, 2318 (2021).
[35] E. Spohr, Electrochim. Acta **44**, 1697 (1999).
[36] Z. Bo, H. Yang, S. Zhang, J. Yang, J. Yan, and K. Cen, Sci. Rep. **5**, 14652 (2015).
[37] O. J. Lanning and P. A. Madden, J. Phys. Chem. B **108**, 11069 (2004).
[38] G. Feng, J. Huang, B. G. Sumpter, V. Meunier, and R. Qiao, Phys. Chem. Chem. Phys. **12**, 5468 (2010).
[39] J. I. Siepmann and M. Sprik, J. Chem. Phys. **102**, 511 (1995).
[40] S. W. Coles and V. B. Ivaništšev, J. Phys. Chem. C **123**, 3935 (2019).
[41] J. B. Haskins and J. W. Lawson, J. Chem. Phys. **144**, 184707 (2016).
[42] Z. Wang, Y. Yang, D. L. Olmsted, M. Asta, and B. B. Laird, J. Chem. Phys. **141**, 184102 (2014).
[43] J. F. Smalley, C. V. Krishnan, M. Goldman, S. W. Feldberg, and I. Ruzic, J. Electroanal. Chem. Interfacial Electrochem. **248**, 255 (1988).
[44] J. F. Smalley, M. D. Newton, and S. W. Feldberg, Electrochem. Commun. **2**, 832 (2000).
[45] P. Sebastián, R. Martínez-Hincapié, V. Climent, and J. M. Feliu, Electrochim. Acta **228**, 667 (2017).

[46]V. Climent, B. A. Coles, and R. G. Compton, J. Phys. Chem. B **106**, 5258 (2002).
[47]V. Climent, B. A. Coles, R. G. Compton, and J. M. Feliu, J. Electroanal. Chem. **561**, 157 (2004).
[48]H. Zhou, J. H. Park, F.-R. F. Fan, and A. J. Bard, J. Am. Chem. Soc. **134**, 13212 (2012).
[49]A. Trojánek, V. Mareček, and Z. Samec, Electrochem. Commun. **86**, 113 (2018).
[50]A. S. Mogoda, Bull. Mater. Sci. **43**, 100 (2020).
[51]T. Dufils, G. Jeanmairet, B. Rotenberg, M. Sprik, and M. Salanne, Phys. Rev. Lett. **123**, 195501 (2019).
[52]T. Dufils, M. Sprik, and M. Salanne, J. Phys. Chem. Lett. **12**, 4357 (2021).
[53]R. G. Parr and W. Yang, *Density-Functional Theory of Atoms and Molecules* (Oxford University Press, Oxford, New York, 1989).
[54]A. K. Rappe and W. A. Goddard III, J. Phys. Chem. **95**, 3358 (1991).
[55]S. W. Rick, S. J. Stuart, and B. J. Berne, J. Chem. Phys. **101**, 6141 (1994).
[56]D. M. York and W. Yang, J. Chem. Phys. **104**, 159 (1996).
[57]H. Nakano and H. Sato, J. Chem. Phys. **151**, 164123 (2019).
[58]M. Zhang and R. Fournier, J. Mol. Struct.: THEOCHEM **762**, 49 (2006).
[59]M. Zhang and R. Fournier, J. Phys. Chem. A **113**, 3162 (2009).
[60]T. Milek and D. Zahn, Nano Lett. **14**, 4913 (2014).
[61]J. Oshiki, H. Nakano, and H. Sato, J. Chem. Phys. **154**, 144107 (2021).
[62]I.-C. Yeh and M. L. Berkowitz, J. Chem. Phys. **111**, 3155 (1999).
[63]H. Heinz, R. A. Vaia, B. L. Farmer, and R. R. Naik, J. Phys. Chem. C **112**, 17281 (2008).
[64]H. J. C. Berendsen, J. R. Grigera, and T. P. Straatsma, J. Phys. Chem. **91**, 6269 (1987).
[65]M. Patra and M. Karttunen, J. Comput. Chem. **25**, 678 (2004).
[66]A. Morita and S. Kato, J. Chem. Phys. **108**, 6809 (1998).
[67]H. Nakano, T. Yamamoto, and S. Kato, J. Chem. Phys. **132**, 044106 (2010).
[68]J. Caldwell, L. X. Dang, and P. A. Kollman, J. Am. Chem. Soc. **112**, 9144 (1990).
[69]G. Maroulis, *Atoms, Molecules and Clusters in Electric Fields: Theoretical Approaches to the Calculation of Electric Polarizability*, Series in Computational, Numerical, and Mathematical Methods in Sciences and Engineering (Imperial College Press, 2006).
[70]W. G. Hoover, Phys. Rev. A **31**, 1695 (1985).
[71]H. C. Andersen, J. Comput. Phys. **52**, 24 (1983).
[72]W. Smith, T. R. Forester, and I. T. Todorov, *The DL_POLY Classic (1.10) User Manual, CCLRC* (Daresbury Laboratory, Daresbury, Warrington, UK, 2017).
[73]A. P. Willard, S. K. Reed, P. A. Madden, and D. Chandler, Faraday Discuss. **141**, 423 (2009).
[74]D. T. Limmer, C. Merlet, M. Salanne, D. Chandler, P. A. Madden, R. Van Roij, and B. Rotenberg, Phys. Rev. Lett. **111**, 106102 (2013).
[75]V. Raicu and Y. Feldman, *Dielectric Relaxation in Biological Systems: Physical Principles, Methods, and Applications* (Oxford University Press, USA, 2015).
[76]J. Chmiola, G. Yushin, Y. Gogotsi, C. Portet, P. Simon, and P. L. Taberna, Science **313**, 1760 (2006).
[77]J. Vatamanu, O. Borodin, and G. D. Smith, Phys. Chem. Chem. Phys. **12**, 170 (2010).
[78]L. Xing, J. Vatamanu, O. Borodin, and D. Bedrov, J. Phys. Chem. Lett. **4**, 132 (2013).
[79]H. P. Van Leeuwen, Electrochim. Acta **23**, 207 (1978).
[80]A. J. Bard and L. R. Faulkner, *Electrochemical Methods: Fundamentals and Applications* (Wiley, New York, 2001).